UCRL-20591
c.2

RECEIVED
LAWRENCE
RADIATION LABORATORY

LIBRARY AND
DOCUMENTS SECTION

INTERFACIAL DEFECTS IN GALLIUM ARSENIDE DEVICES

Richard A. Osiecki
(M.S. Thesis)

June 1971

AEC Contract No. W-7405-eng-48

LAWRENCE BERKELEY LABORATORY
UNIVERSITY OF CALIFORNIA • BERKELEY

TWO-WEEK LOAN COPY

This is a Library Circulating Copy which may be borrowed for two weeks. For a personal retention copy, call Tech. Info. Division, Ext. 5545

UCRL-20591
c.2

25

DISCLAIMER

This document was prepared as an account of work sponsored by the United States Government. While this document is believed to contain correct information, neither the United States Government nor any agency thereof, nor the Regents of the University of California, nor any of their employees, makes any warranty, express or implied, or assumes any legal responsibility for the accuracy, completeness, or usefulness of any information, apparatus, product, or process disclosed, or represents that its use would not infringe privately owned rights. Reference herein to any specific commercial product, process, or service by its trade name, trademark, manufacturer, or otherwise, does not necessarily constitute or imply its endorsement, recommendation, or favoring by the United States Government or any agency thereof, or the Regents of the University of California. The views and opinions of authors expressed herein do not necessarily state or reflect those of the United States Government or any agency thereof or the Regents of the University of California.

Table of Contents

Abstract v
Introduction 1
Experimental 7
Discussion 17
Summary 24
Acknowledgment 25
References 26
Figure Captions 28
Figures 30
Appendix 50

INTERFACIAL DEFECTS IN GALLIUM ARSENIDE DEVICES

Richard A. Osiecki

Inorganic Materials Research Division, Lawrence Radiation Laboratory
Department of Materials Science and Engineering, College of Engineering
University of California, Berkeley, California

ABSTRACT

Defects in the interfacial regions of a gallium arsenide pulse generating device have been observed. These consisted of silicon and other impurity inclusions and/or dislocation arrays. The defects were detected at the free surface, the epitaxial/epitaxial interface region, and the epitaxial/substrate interface region. A model based upon an impurity rich deposit/gallium arsenide pair is proposed to explain the observed defects.

The research was done using a 650kV electron microscope.

INTRODUCTION

GaAs is a semi-conducting material which exhibits a potentially useful electrical characteristic, i.e. negative resistivity,* [1] which may have many applications, one of which is a pulse generating device (see Fig. 2). However, this device has not achieved its potential because of electrical breakdown in the interfacial (junction) regions. Computer simulation has shown that the breakdown behavior can be caused by the presence of "i" or "p" (insulating or positive carrier) anomalous layers in the interfacial region. The presence of these layers has been observed by scanning electron microscopic examination of cleaved and etched edges of the devices,[2] however direct transmission electron microscopic observation of these has not been achieved.

There are several reasons for the difficulties in observing the interfacial regions in the electron microscope. The first of these is the difficulty of chemically thinning GaAs to transparency for electron microscopic examination. Ion milling machines have alleviated this problem somewhat but the use of these machines is not yet widespread. The second problem is the sampling problem, that is, the low probability that localized defects, such as small impurity layers at the interfaces, would be present in a foil thin enough to be observed in the electron microscope.

Fortunately, these problems are not insurmountable. A chemical means of successfully polishing this material has been developed and will be described later. The second problem was reduced by using the Berkeley HU650 high voltage electron microscope. Because of the higher energy electrons, thicker specimens can be observed (in practice, specimens up to 4 microns were observed whereas observation is limited to

*See Appendix.

approximately 1 micron in 100 kV microscopes). This increased useful foil thickness greatly increased the volume of sample observed, increasing the probability that defects would be found. Also HVEM allows, because of multibeam interaction, the use of some experimental techniques which aid in the imaging of defects.

Review of Interfacial Defects in Semi-Conducting Defects

There are two distinct categories of origin into which defects at the interface may be divided, those which are inherent to the device, e.g., misfit dislocations caused by the different lattice parameters of the regions doped to different levels, and those which are a product or result of the fabrication technique, e.g. oxides or other deposits at the free surface or the interfaces. Since both of these defects may exhibit detrimental electrical properties, knowledge of these is important for successful device design.

Elemental semi-conductors, e.g. Si, have the diamond cubic structure while the compound semi-conductors, such as the III-V compound GaAs, have the sphalerite structure (see Fig. 1). The dislocation structure which is present in these structures has been discussed by Hornstra.[3] The Burgers vector is $a/2\langle 110\rangle$ and slip takes place on the $\{111\}$.[4] Electrical characteristics of dislocations have been reviewed by Friedel.[5]

There are two basic means of producing the different levels of doping required for semi-conductor operation, the diffusion of the dopant into the substrate and the growth, either from the vapor or from the liquid, of the doped layer onto the substrate. In either case, characteristic misfit dislocation networks result. Levine et al.[6] have observed the dislocations which result from the diffusion of the dopant into the substrate and Tamura and Sugita[7] observed the dislocations which are present at the interface of vapor deposited epitaxial layers.

In both cases, a network of dislocations formed from stress induced slip dislocations. This network then accommodated the stress caused by the mismatch of lattices across the interface.

Direct observations of the second type of defect are not so prevalent. Thomas[8] has shown the formation of stacking faults from inclusions at the interface in a Si device. Indirect observations, e.g. by thermal methods,[9] have shown the presence of inclusion or surface deposits in semi-conducting devices and the effect these have on electrical performance. Also the presence of defects has been indicated by electrical characteristics as mentioned earlier.

The GaAs devices used in this study were prepared by vapor deposition and/or solution growth of the doped layers. Because of the low doping levels involved, there is little mismatch of the lattices across the interface. (Assuming Vegard's law is spplicable, the spacing of misfit dislocations would be on the order of 10's of μm.) Thus, at best, only a small number and apparently "stray" misfit type dislocations should be observed. However, there is the evidence that anomalous layers are present at the interface. Thus, the problem in this study is to locate and characterize these localized, randomly distributed interfacial defects.

Specimen Fabrication

The GaAs devices were supplied in the as-grown condition. Devices in which the n^+ layer was vapor deposited and solution grown were provided by Texas Instrument, Inc. A typical device configuration is shown in Fig. 2.

The substrate is a Czochralski grown single crystal of GaAs, grown in the [001]. This is doped with either Te or Si to approximately $5 \cdot 10^{18}$ e^-/cc. The n^- layer is vapor deposited and doped to the lowest

possible level consistent with the fabrication technique, in this case about 10^{15} e^-/cc. The n^+ layer is either vapor (gas to solid reaction) deposited or solution (liquid to solid reaction) grown. Vapor deposition takes place at 750°C,[10] while the solution growth takes place at approximately 1240°C.

Specimen Preparation and Experimental Procedure

The devices were received in the form of wafers, approximately 0.5 mm thick and from 1 cm to 3 cm across. The epitaxially deposited surfaces were extremely flat and mirrorlike while the reverse surfaces exhibited many regularly spaced saw marks, probably caused by a diamond saw.

A number of these were then mechanically thinned to approximately 175 microns, the last 25 microns being removed with 1 micron diamond paste. These were chemically thinned to transparency, as needed. Other specimens were thinned to transparency completely by chemical means. No difference in the foil condition could be discerned between these methods.

Two basically different experiments were performed. One was an etching experiment to detect dislocations intersecting the surface and the other was the microscopic examination.

The etching experiments are rather easily performed. A small (5×5 mm) chip of GaAs is mounted, expitaxial face up, on a glass slide, using Apiezon wax. The surface is then exposed to the etchant, or polish and then etchant, for short periods of time. The surface is observed optically at up to 600 times magnification and micrographs of the surface are taken if desired. By repeating the polish/etch sequence, a depth profile of dislocation location can be obtained. The polish/etch sequence consists of an approximate 3 seconds immersion in the polishing

solution, rinse in water, followed by a 4 sec exposure to the etchant, rinsing in water, washing with ethyl alcohol and drying. Each polish/etch cycle removes slightly less than 0.5 μm of material.

The etchant consists of 2 ml H_2O, 8 mg $AgNO_3$, 1 g CrO_3 and 1 ml HF.[11]

The polishing solution consists of 20 parts H_3PO_4, 1 part HF and 1 part HNO_3 (all by volume). A small polyurethane beaker containing the solution is placed in a container of water heated to 60°C. The solution is constantly stirred by a magnetic stirrer, since stirring action constantly washes the specimen surface, reducing any tendency to form pits. Also the stirring helps to maintain thermal equilibrium in the solution.

In order to thin a specimen that has the interfacial region within the transparent region, it is necessary to know where the interface is. This is accomplished by observing the cleaved edge (all specimens are reduced to proper size by cleaving) after etching that edge for about 8 seconds. The etchant reveals the interfaces (see Fig. 3). Then, by short immersions of the specimen in the polishing solution and re-observing the distance of the desired interface from the free surface, it is possible to locate that interface within one or two microns of the free surface. The specimen (2-4 mm on a side) is then mounted epitaxial face down on a slightly larger glass chip with Apiezon wax. The chip is placed in the polishing solution and allowed to thin. The rate of thinning is approximately 4 microns/min. When a hole forms within the specimen, or when one dimension of the specimen is reduced by 50%, the specimen is removed from the solution and rinsed in water. The wax is then dissolved by trichloroethylene. The specimen is rinsed in acetone, ethyl alcohol and, finally, floated on distilled water. If proper care is taken (GaAs is fragile), a foil with transparent (both to light and electrons) areas is obtained. The foil is ready then to mount in the

specimen holder and be observed in the microscope.

Transmission microscopy was performed on a Hitachi HU650 electron microscope, operated at 650 kV. Microprobe work was done on a Materials Analysis Company Electron Microprobe Analyzer Model 400-S.

EXPERIMENTAL

Figure 4 illustrates the convention followed in the indexing of the micrographs to be presented. Because all foils will have either the [001] normal of [00$\bar{1}$] pointing toward the electron gun when viewed in the microscope, defects may be viewed either from the "bottom" (down the [00$\bar{1}$] or from the "top" (down the [001]). In cases where the defect/matrix orientation relation is known, as at the free surface, the foil normal can be determined. In other cases where the normal cannot be determined, as at the epitaxial/epitaxial region, the position of the line of intersection of the slip planes will be the determining factor. If it is at the bottom (as determined by stereomicroscopy or comparison of bright field and dark field images) of the foil, a [00$\bar{1}$] normal is at the top of the foil, a [001] normal is assumed. The line of intersection, since it always lies along a ⟨110⟩ in the (001), will always be said to lie along the [110]. This convention will allow consistent directions, Burgers vectors and slip planes to be assigned to the dislocations observed, whether viewed from the "top" or "bottom." This convention, however, tacitly suggests that the arrays always project into the matrix, away from the free surface. While this is necessarily true for the defects found at the free surface, this suggestion cannot be verified for the defects in the epitaxial/epitaxial region.

The normal of each figure will be given in the figure caption when necessary.

Microscopic-Free Surface

An examination of the free surface was undertaken for two reasons: 1) it is the easiest "interface" to isolate in a thin foil, and 2) since the vapor deposited n^+ layers are formed by the same methods that the n^- layers were formed, the condition of this interface in the as-received

condition will approximate the n^- layer at the end of its fabrication.

Several types of defects were observed. A scratch which occurred during handling is shown in Fig. 5. Although not caused by a fabrication technique and therefore not a "typical" defect, it is shown for reasons of comparison to the other defects observed. This figure was taken on a Hitachi HU125, operating at 125 kV. Other defects are in Figs. 6 and 7. It can be seen in Fig. 6 that the dislocation array did not form on a scratch or other obvious mechanical defect. The dislocations form loops which extend into the matrix from the bottom surface of the foil (which corresponds to the initial free surface of the foil).

Figures 6a-d are a series of $\bar{g}\cdot\bar{b}$ experiments to determine the Burgers vector of the dislocations. Because of the [001] orientation of the foil and limitations of the tilting device (± 14°, which does not allow enough tilt to tilt the foil to a reflection strong enough to determine the sign of the third digit of the Burgers vector direction), the third digit has to be determined by indirect means. One set of dislocations are out of contrast for g = [040] while the others are out of contrast for g = [400] indicating that the Burgers vectors are $a/2[\bar{1}01]$ and $a/2[0\bar{1}1]$ respectively. A point to note in Figs. 6b and 6d is that the segments of the out of contrast dislocations which lie along the [$\bar{1}$10], exhibit residual contrast while the segments which run through the foil along the [0$\bar{1}$1] and [101] exhibit none. This residual contrast is indicative of dislocations with edge components.[12] Figure 6e and 6f are micrographs with higher order reflections of those in Fig. 6b and Fig. 6d operative. It should be noted that the residual contrast is not present, while the in contrast dislocations are. This is due to the weaker diffracting conditions of this reflection.[13] The $\bar{g}\cdot\bar{b}$ analysis of these dislocations indicated that the Burgers vector is a/2[011] or

$a/2[0\bar{1}1]$ and $a/2[101]$ or $a/2[101]$ respectively. Since the segments of these dislocations which intersect the surface lie along $[0\bar{1}1]$ and $[101]$ respectively, these segments are in either pure screw or pure edge orientation, but because of the lack of residual contrast from these segments, it is concluded that these segments must be in screw orientation. The $[\bar{4}\bar{4}0]$ and $[\bar{4}\bar{4}0]$ reflections were used instead of $[\bar{2}\bar{2}0]$ and $[\bar{2}20]$ in Fig. 6a and Fig. 6c because of the increased resolution possible with these higher order reflections.[14]

Figure 7 is of another defect found emanating from the free surface. It is a "butterfly" of dislocations which is formed by dislocations lying along $[\bar{1}0\bar{1}]$ and $[01\bar{1}]$. Once again residual contrast is present from the $[1\bar{1}0]$ and $[110]$ segments of the out-of-contrast dislocations in Fig. 7d, indicating that these have edge components (compare the arrowed regions in Figs. 7c and 7d). The $\bar{g}\cdot\bar{b}$ analysis of this array indicates the Burgers vector is $a/2[101]$ or $a/2[10\bar{1}]$ while it is $a/2[011]$ or $a/2[01\bar{1}]$ for those oriented along the $[01\bar{1}]$, but since the segments which lie along these directions have no edge components, the long segments are in screw orientation. Figure 7e is a displaced aperture dark field micrograph of the same array. Because of the reversal in black/white at the bottom of the foil (which corresponds to the free surface and the intersection axis of the slip planes), the areas which are blackened out in Fig. 7a are visible in Fig. 7e. It can be seen in this figure that the origin of these dislocations does not appear to be a scratch or other obviously mechanical defect.

The non-screw dislocation segments lie along the $[\bar{1}10]$ in Fig. 6 and along the $[\bar{1}10]$ and $[110]$ in Fig. 7. Since the Burgers vector, screw, and non-screw segments lie in common $\{111\}$, the dislocations are in a glide configuration. Only two slip planes, the (111) and $(\bar{1}\bar{1}1)$ are

operative in Fig. 6 and three are operative, the (111), $(\bar{1}\bar{1}1)$ and $(\bar{1}11)$ in Fig. 7. There are two points of similarity to be pointed out in these two defects: 1) the long dimension of the array in both cases is along a $[\bar{1}10]$, and 2) the dislocations are in glide configuration.

Microscopic Epi-Epi Interface

Attempts to study the epi-epi interface were more difficult than the free surface because of the greater difficulty in isolating the interface in a thin foil. Although the cleaved edges could be observed and sufficient surface material removed so that the interface was within one or two microns of the free surface at the edge, there was some uncertainty as to the location of the interface at the point that subsequently became transparent. This uncertainty arose from the unevenness of material removed by the polish and the fact that the interface was not necessarily parallel to the free surface. In addition, there was also the problem that the defects which were being sought were not uniformly distributed but occurred in localized areas. The uncertainty of the relation of the interface to the foil led to some difficulty in the interpretation of the defects to the interface. That is, was the defect above, below, or at the interface, did the defect extend into the matrix on both sides of the interface or just one?

Figure 8 shows a dislocation array found in the epi-epi region of a device in which the n^+ layer was solution grown. By using a 10° wedge in the specimen holder, it was possible to obtain the $g = [\bar{1}31]$ reflection shown. This shows that the Burgers vector of the dislocations out of contrast in Fig. 8b is $a/2[101]$. Since this set of dislocations lies along the $[101]$, this set is in the screw orientation. Because of foil contamination, it was impossible to obtain the necessary reflections to determine the Burgers vector of the other set. However, the

reflection which was obtained shows the Burgers vector to be either $a/2[011]$ or $a/2[0\bar{1}1]$. Because the through-the-foil dislocations lie along the $[0\bar{1}1]$ and because of the lack of residual contrast, indicating no edge components it is concluded that the Burgers vector is $a/2[0\bar{1}1]$. It should be noted that the dislocations do not appear to originate on any obvious source. Also the dislocations are in glide configurations forming dipoles, as are those found at the free surface.

Figure 9 is of an array found in the epi-epi region of a device with the n^+ layer vapor deposited. By the $\bar{g}\cdot\bar{b}$ analysis and residual contrast arguments used earlier, it is determined that these are the same type of dislocations discussed earlier. Perhaps the significance of this array is the reduced foil thickness at the axis of the array. This can be explained if an impurity was present and then etched out by the polish, leaving the reduced foil thickness at the center and the dislocations at the periphery. Figure 10 is a stereographic pair of this array. From this figure it is possible to see that the dislocations do not emanate on a single slip plane but rather on two sets of slip planes. These planes are the $(\bar{1}\bar{1}1)$ and $(\bar{1}11)$ since the non-screw segments lie in the $[110]$ and $[1\bar{1}0]$. Figure 11 is a low magnification micrograph of the same area showing two of these arrays existing close to each other.

Figures 12, 13 and 14 are figures which further illustrate details of arrays of the type shown above. Figure 12 is of dislocations completely through the foil, apparently caused by two sources outside the foil while figures 13 and 14 further illustrate points mentioned earlier. The Burgers vector analysis yields the same result as the arrays shown

earlier. (Of course, it is impossible to see any residual contrast in Fig. 12 because there are no edge components present in the foil.) The ridges which show up in Fig. 12 (arrows) are thought to be surface effects. Figure 13 shows dislocations on two parallel slip planes. The dislocations of both planes go through the foil in the same direction (that is both are along the $[\bar{1}0\bar{1}]$, not one along the $[\bar{1}0\bar{1}]$ and one along the $[\bar{1}01]$). Note the residual contrast in Fig. 13b, which is consistent with the other arrays shown. Figure 14 is of an array taken with the specimen in the 10° wedge specimen holder. Since the beam is now closer to being perpendicular to one of the slip planes, (because the foil in the normal specimen holder is always [001] and the dislocations are on {111}, they are always viewed at between 50° and 60°), the array projects a much wider top of foil to bottom of foil image, revealing more clearly the edge components of the arrays.

Figure 15 further illustrates the effect of higher order reflections on image resolution mentioned earlier. By placing higher order reflections on the Ewald sphere (s=0) it is possible to obtain higher image resolution or less image confusion, thus allowing the easier interpretation of dislocation configuration. This technique has proved useful in the study of defects of this type.

Microscopic-Substrate-Epitaxial

The study of this region did not reveal defects of the type found in the other interfacial regions. There are three possible reasons for this: 1) The number of defects is lower, reducing the probability of finding a defect in the thin foil, 2) the defects are not present, or 3) the problems mentioned in trying to find the epitaxial-epitaxial interface are increased by the increased depth of this interface thereby lowering the probability of finding an interface. It is not certain

which of these is correct, however, defects were detected in this region by electrical means so it must be assumed that the second reason above is not applicable.

Polish/Etch

The arrays found by microscopy, because they are not parallel to the foil surface, are easily detectable by polish/etch means. Individual dislocations in the arrays would not be distinguishable because of the very close spacing of the dislocations, however, the cumulative effect of all the dislocations in an array would be noticeable. An array should show up as a linear etch pit (a pit in which that one dimension is more than twice the one at 90° to it) and lie along a ⟨110⟩ which lies in the (001). An advantage of this method is that since the surface is examined by optical means, it is possible to observe macroscopic areas, allowing the determination of the length of the arrays, the distribution of the arrays, and possibly, the origin of the arrays.

Figure 16 is of the free surface, the epitaxial-epitaxial region and the substrate-epitaxial region, A, B, and C respectively. In each of these the linear etch pits are present. It is estimated that they have a maximum length of 10 microns. Exact size determination of an array is difficult because an etch pit is seen, not the array itself. At all three levels the pits lie along a ⟨110⟩. This orientation can be determined by X-ray analysis or by comparing the direction of etch pit with the cleaved edge of the specimen. Since GaAs cleaves on a {110}, the cleaved edge will be along a ⟨110⟩, thus the etch pits should always lie parallel to or perpendicular to an edge if they are along a ⟨110⟩ in the (001). Orientation was determined by both means at first and then only by the latter when the early results were consistent with each other. The density of these pits is very high in this particular

specimen, which was found to also have a fairly high density of Si particles. This density of pits was not normally observed, as subsequent figures will show this. It is not understood why all the particles in a given region lie along the same ⟨110⟩, that is, if the formation of the arrays was completely random, arrays should form along both the [110] and [$\bar{1}$10].

Figure 17 is a series of optical micrographs taken of the same area at different levels of the specimen. A is within 1/2 micron of the free surface, there are not etch pits present, but there is an inclusion (arrow) on the surface. B and C are taken at increased (0.4 microns and 4.0 microns respectively) from the original free surface. It can be seen that the etch pits similar to those noticed earlier have developed at the site of the inclusion. A similar series of micrographs, of a different specimen, are shown in Fig. 18.

Since the arrays were formed from inclusions which were evident on the free surface, an X-ray microprobe survey of the free surface should identify the composition of the inclusion. The initial survey was done on two specimens, one in the as-received condition, the other after one polish/etch cycle. Both specimens were rinsed with ethyl alcohol prior to observation. The probe of the unetched specimen revealed a few small silicon concentrations while the probe of the etched specimen revealed many silicon deposits, as if silicon deposits were present immediately below the free surface. (Other etched specimens did not reveal large numbers of silicon particles indicating that the number of silicon particles changed from specimen to specimen. The silicon could not have been from the polishing or etching solutions as no appreciable amount of glass or other source of silicon was present in the solution.) Figure 19A is a SiK_{α}, X-ray trace of the surface shown in Fig. 19B. There is

a correspondence between the silicon concentrations and particle position although not all particles correspond to silicon concentrations. These latter particles have not been identified although it is known that they are not silicon or tellurium. The surface irregularities present in Fig. 19B are an artifact from the polish/etch cycle.

Figure 20A is of a specimen which showed a high Si particle concentration in the area shown in the micrograph. Figures 20B and C are taken at deeper levels, B being about 0.5 μm deeper than A and C about 3.5 microns deeper. There are many etch pits evident in C. D is a micrograph of an area immediately adjacent to C. Some etch pits are evident here but the density is much lower, D is more typical of most specimen surfaces than Figs. 16 or 20C. The source of the gross surface defect evident in B is unknown. It appears that at the time of initial deposition of the final layer, a layer of noncrystalline or non-"sticking" material was deposited and then covered by the GaAs layer. Then, when the surface was removed, it became evident once again. This correlation of high silicon concentration and high etch pit density further indicates that the dislocation arrays are associated with silicon deposits. Note that all the etch pits in this area lie along the same ⟨110⟩.

Although this method proved useful in determining a possible origin of the dislocation arrays as well as the distribution of them, it is subject to some shortcomings. Perhaps the greatest of these is that a pit may be "remembered" after the dislocations have been polished away. This adds confusion as to which level the pit originally formed as well as the cumulative effect of pits, that is, as more and more of the surface is washed away, the apparent density of the arrays may seem higher than it actually is. Another fault is that the amount of material removed can only be estimated, preventing the exact determination of

of depth at which a pit formed.

Table I gives the method of deposition of the n^+ layer for each of the figures. It can be seen that there is no correlation between the type defect observed and the method of deposition of this layer. The defects are common to both means of epitaxial growth.

Table I

Figure	Method of deposition of n^+ layer
6	V
7	V
8	S
9	V
10	V
11	V
12	S
13	S
14	V
15	S
16	V
17	V
18	V
19	V
20	V

V = vapor deposited
S = solution grown

DISCUSSION

Two related defects were observed in the interfacial regions: 1) impurity deposits, and 2) dislocation arrays, associated with the deposits. Some of the deposits were silicon or silicon rich while others were not identified. These were found at the free surface and their effects (dislocation arrays) were observed in the interfacial regions. Associated with the deposits were dislocation arrays which consisted of glide dislocations on two intersecting {111}. The area of intersection was characterized by a dislocation "tangle." These defects were randomly distributed throughout the plane of the interface with the matrix immediately adjoining the deposits and arrays being essentially dislocation free.

These dislocation arrays are not of the type which would accommodate the mismatch of the differently doped GaAs matrices present in these devices. The Burgers vectors do not lie in the (001), as would be expected if these were "normal" misfit dislocations, the arrays are much too localized to account for a general misfit phenomenon, the dislocations form screw dislocation dipoles which do not effectively relieve strain, and the density of the dislocations in the "arrays" is much too high to relieve misfit between two lattices based upon the gallium arsenide matrix.

Although the "tangle" cannot be composed of misfit dislocations between doped and undoped gallium arsenide, it may be the result of misfit between gallium arsenide and some other materials.

One such material is silicon. Silicon was observed as an inclusion in these devices although other unidentified inclusions were also found. Based on the relation[15]

$$P = \frac{ab}{|(a-b)|}$$

where P = misfit dislocation spacing

a, b = appropriate planar spacing of lattices involved.

The misfit dislocation spacing in a gallium arsenide/silicon interface would be on the order of 150 Å. It is doubltful that pure silicon deposits are present in this material, but silicon rich deposits are possible and have been observed.[16] The spacing of dislocations caused by the presence of silicon in a gallium arsenide matrix would be dependent upon the amount of silicon present. The closest spacing would be of the order mentioned above, and would get progressively greater as the atomic fraction of silicon decreases.

The model being proposed is that during the fabrication process semi-coherent, impurity rich deposits form in the interfacial regions of the gallium arsenide device. The semi-coherent interfaces could be expected to lie in {111} with the misfit dislocations and Burgers vectors in these planes. The dislocations would be glissile, subject to thermal stresses which form at the matrix/deposit interface during the cooling of the device from fabrication temperature and would glide. These stresses arise from the different amounts of contraction of the impurity deposit and gallium arsenide matrix.

The stress, if not relieved by the slip of the misfit dislocations, could also "punch out" stress relieving dislocations directly. The gliding dislocations would remain connected to the deposit/matrix interface by dislocation segments, forming the observed dipoles. These form the "butterflies" which are observed experimentally.

One of the assumptions of the proposed model is that the interface between the deposit and the matrix lies along a {111} or rather, on a

series of parallel {111}, since it is doubtful that the interface would be a single plane. (For ease of presentation, however, the interface will be treated as a well defined deposit/matrix interface.) This assumption is justifiable for several reasons. The first of these is that each of these planes contain three of the "habit" ⟨110⟩ which dislocations in this material lie along as well as the direction of the Burgers vector. Hence, a complete network of misfit dislocations is more easily "created" in these planes than in other planes. A second reason is the layered structure peculiar to the sphalerite structure.[17] The {111} are not equally spaced, that is, the distance from the (111) gallium plane to the arsenic plane in the [111] is less than the distance to the arsenic plane in the $[\bar{1}\bar{1}\bar{1}]$ (see Fig. 22). Thus the sphalerite structure is "layered" along the ⟨111⟩, each layer consisting of one plane of gallium and one plane of arsenic. By replacing one such layer with two planes of silicon (which maintains electronic as well as atomic balance), the angular distortion of the bond between the silicon atom and neighboring gallium or arsenic atom, because it involves only one, "long" bond, per silicon atom, is minimized reducing the "electronic surface energy" of this interface. Figure 23 shows two possible configurations for the bottom of the deposit. A is a single "trough" formed by two {111} planes, and B is a "sawtooth" effect consisting of many small troughs formed by {111} planes. The dashed lines are projections of these planes into the gallium arsenide matrix.

The dislocations which lie in these planes lie along the three ⟨110⟩ in each plane. The combinations of the ⟨110⟩ "habit" directions of the dislocations and the possible Burgers vectors produce either 60° dislocations or pure screw dislocations. Because of the mismatch nature of these dislocations, it is expected that the former would predominate.

Both of these types of dislocations are glissile and, hence, can glide upon the application of a stress. As the length of dislocation moves out from the deposit/matrix interfacial area regions it would "leave behind" a dislocation to this region. It can be expected that it would be easier for glissile dislocations to glide so that the residual dislocation is in screw orientation rather than non-screw orientation as there are no broken or unsatisfied bonds in the core of a screw dislocation as can occur for a non-screw dislocation.[18] These would form the dislocation dipoles which were observed.

Another assumption of this model is that a stress is induced by the cooling of the device to room temperature. This stress would be caused by different amounts of contraction of the deposit and the matrix. The coefficients of thermal expansion for silicon and gallium arsenide are $7.36 \cdot 10^{-6}$ cm/cm°C and $5.93 \cdot 10^{-6}$ cm/cm°C, respectively. This difference in coefficients should be sufficient to produce the stresses necessary to cause glissile dislocations to glide into the matrix, relieving the stress. This stress has been calculated to be of the order of 10^6 dynes/cm^2 for a pure silicon/gallium arsenide interface and with no stress relief by dislocation glide. The stress would obviously be less for a couple in which the deposit was less than pure silicon.

The final dislocation array configuration would, of course, depend on the amount of impurity in the deposit, the higher the atomic fraction of impurity in the deposit the greater the thermal stresses and the greater the amount of glide and/or the number of dislocations involved.

Defects with apparent different amounts of impurity have been observed. Figure 6 is of an array at the free surface in which a relatively small amount of silicon, or other impurity, deposited. The number of dislocations is relatively small and have a glide a relatively

short distance. In Fig. 7, apparently a relatively large amount of impurity is present with the result that dislocations are more numerous and have glided a greater distance than those in Fig. 6.

It would be expected that deposits in the epitaxial/epitaxial region would be larger, with the result that the arrays will consist of a greater number of dislocations or the dislocations would have slipped a greater distance. Figure 8 illustrates the latter point while Fig. 9 illustrates the former. Figure 12 is of dislocations completely through the foil, indicating that the dislocations have glided a relatively large distance, indicating the deposit is large.

It is difficult to determine which mechanism of formation is operative. In Fig. 8 it appears that the dislocations were punched out on a limited number of slip planes while Fig. 9 appears as if a large number of essentially randomly distributed dislocations slipped a short distance. Both mechanisms can apparently operate, depending on the geometry of the deposit.

These silicon rich deposits would be difficult to detect since they would consist of semi-coherent regions with only a slight change in the lattice constant of that region (proportional to the atomic fraction of the silicon). Hence, additional spots would appear only faintly and only slightly off of the strong, main matrix spots. This lattice strain would be noticeable as strong strain contrast at the surfaces of the foil. This is observed in Figs. 7 and 8 as dark areas in the central region of the array (this contrast is reversed in the dark field image in Fig. 7E). In addition to these, it is also possible that the silicon was etched away by the polish, as it was in Fig. 9.

This model explains why the dislocation arrays form, but only by assuming that silicon or any other impurity/segregate deposits are

present. It does not provide a mechanism for the formation of these deposits, which is beyond the scope of this project. A coordinated program in which access to material at all stages of fabrication, as well as control of the fabrication techniques, is necessary to answer this question.

One of the most puzzling things to be answered about these defects is the fact that they always lie along a ⟨110⟩. This would be expected if the "walls" of the deposit had to be {111} which would automatically cause the array to lie along the ⟨110⟩, but this is a weak argument. It may be that these deposits nucleate and grow on the misfit dislocations which form between the gallium arsenide doped and undoped regions. Since these would lie along ⟨110⟩, the deposit would naturally lie along ⟨110⟩. Another possibility is that it is easier for a deposit, once it has nucleated on some surface imperfection, to grow in a ⟨110⟩ because this is the "habit" direction of dislocations. That is, it would be easiest for misfit dislocations to accommodate the deposit if the deposit formed along a ⟨110⟩.

Also why are only a limited number of slip systems operative, is there an orientation relation between the deposit/matrix in which certain slip systems are more favorably aligned than others? And a final question is why do all the arrays in a given area lie along the same ⟨110⟩, it would be expected that the arrays would be aligned in approximately equal number between the [110] and [1$\bar{1}$0].

One last point to mention is that once a "seed crystal" of the impurity has formed and is growing, presumably along a ⟨110⟩, one of two things can happen. The deposit can continue to grow into an inclusion or the deposit can not grow quickly enough, being covered by the depositing gallium arsenide. Both of these seem to have occurred. Figures

17 and 18 show inclusions which mark sites of the arrays while Fig. 20 shows an instance in which the impurity rich area was improperly covered by the gallium arsenide.

SUMMARY

Impurity inclusions, impurity rich areas and associated dislocation arrays were observed in the interfacial regions in the gallium arsenide devices used in this study. These were observed by electron microscopic means, optical microscopic means and by the electron microprobe. These were found at the free surface, the epitaxial/epitaxial region and the epitaxial/substrate region.

The dislocation arrays consisted of long dislocation loops, in glide configuration, emanating on {111} which intersected along a common ⟨110⟩. It was shown that these arrays could not be the result of the mismatch between the differently doped regions of the gallium arsenide matrix.

A model was proposed to explain the observed dislocation arrays. This model consisted of dislocations gliding under the influence of thermal stresses from the deposit/matrix interface region. There were two sources of dislocations considered, the misfit dislocations which form at the interfacial areas of the deposit/matrix and a "punching out" mechanism in which dislocations were formed directly by the stress. These then glide on favorably oriented slip planes and form the observed loops. It was not determined which mechanism is the more important.

This work identifies the defects found in this region but do not determine the source. A coordinated program with control of the fabrication process is necessary before this can be done.

ACKNOWLEDGMENTS

The author is deeply grateful to Professor Gareth Thomas for his support and guidance throughout the course of this work. He is also grateful to Ron Cox of Texas Instrument, Inc. for supplying the gallium arsenide devices used in this study. Special thanks are due to Don Jurica for his work in maintaining the HU650 and to George Georgakopoulos for performing the electron microprobe analysis.

This work was done under the auspices of the U. S. Atomic Energy Commission through the Inorganic Materials Research Division of Lawrence Radiation Laboratory.

REFERENCES

1. J. A. Copeland, IEEE Spectrum 4 (No. 5) 71 (1967).
2. T. G. Blocker, R. H. Cox and T. E. Hasty, Solid State Commun. 8 (16) 1313 (1970).
3. J. Hornstra, J. Phys. Chem. Solids 5, 129 (1958).
4. J. P. Hirth and J. Lothe, Theory of Dislocations (McGraw Hill, New York, 1968) p. 355.
5. J. Friedel, Dislocations (Addison-Wesley, Reading, Mass., 1967) p. 427.
6. E. Levine, J. Washburn, and G. Thomas, J. Appl. Phys. 38 (1), 81 (1967).
7. M. Tamura and Y. Sugita, J. Appl. Phys. 9 (4), 368 (1970).
8. G. Thomas, Phil. Mag. 17, 1097 (1968).
9. A. Tretola and J. Irvin, J. Appl. Phys. 39, 3563 (1968).
10. E. W. Mehal and G. R. Cronin, Electro. Chem. Tech. 4, 540 (1966).
11. M. Abrahams and C. Buioic hi, J. Appl. Phys. 36, 2855 (1965).
12. P. B. Hirsch, et al.,Electron Microscopy of Thin Crystals (Butterworths, London) (Reprinted, 1969) p. 178.
13. W. Bell, private communication.
14. R. Osiecki and G. Thomas, Proceedings of 29th EMSA Conf. 1971 (to be published).
15. J. H. van der Merwe, Single Crystal Film, (edited by M. H. Francombe and H. Sato) (Macmillan, New York, 1964) p. 139.
16. W. Kern, J. Electrochemical Society 109, 700 (1962).
17. D. B. Holt, J. Phys. Chem. Solids 27, 1053 (1966).
18. J. Hornstra, J. Phys. Chem. Solids 5, 129 (1958).
19. C. R. C. Handbook of Chemistry and Physics, 43rd Edition.
20. J. A. Amick, Single Crystal Film (edited by M. H. Francombe and

H. Sato) (Macmillan, New York 1966) p. 283.

21. C. Kittel, Introduction to Solid State Physics, 3rd edition (John Wiley, New York, 1967) p. 30.

FIGURE CAPTIONS

Fig. 1. The sphalerite structure (after Kittel[21]).

Fig. 2. Schematic of a gallium arsenide pulse generating device.

Fig. 3. (110) edge of a device produced by cleavage. Etching reveals the interfaces.

Fig. 4. Line drawings of the convention followed when indexing observed arrays.

Fig. 5. Surface scratch observed in a gallium arsenide foil.

Fig. 6. Small dislocation loops observed at the free surface of a vapor deposited n^+ layer. Foil normal is $[00\bar{1}]$.

Fig. 7. Dislocation "butterfly" observed emanating from the free surface of a vapor deposited n^+ layer. Arrows in c and d point out residual contrast from edge components of dislocations. Foil normal is $[00\bar{1}]$.

Fig. 8. "Butterfly" observed in the epitaxial/epitaxial interfacial region in which the n^+ layer was solution grown. Foil normal is $[00\bar{1}]$.

Fig. 9. "Butterfly" observed in the epitaxial/epitaxial interfacial region in which the n^+ layer was vapor deposited. Foil normal is $[00\bar{1}]$.

Fig. 10. Stereo pair of array in Fig. 9.

Fig. 11. Low magnification of the region of Fig. 9 showing two of these deposit/arrays existing near one another.

Fig. 12. Screw segments of dislocation arrays from two deposit/array defects extending completely through the foil. Arrowed defects are surface defects, not dislocations.

Fig. 13. Dislocations of one wing of the "butterfly" showing screw and non-screw dislocation on two parallel slip planes.

Fig. 14. One wing of the "butterfly" highlighting the non-screw segments of the dislocations.

Fig. 15. Series of micrographs illustrating the effect of systematic high order reflections at the Bragg condition. Note the image narrowing and reduction of oscillatory contrast of the dislocations which produces a more easily resolvable array. This array is the same array shown in Fig. 13.

Fig. 16. Polish/etch surface showing the linear etch pits produced by the dislocation array observed in the electron microscope. A, B, and C are taken at the free surface, epitaxial/epitaxial region, and epitaxial/substrate regions respectively.

Fig. 17. Series of pictures showing the development of a linear etch pit from an inclusion as surface material is removed.

Fig. 18. Same type of sequence as Fig. 17 but of a different sample.

Fig. 19. A Si K_α x-ray trace and scanning electron micrograph of the same area revealing silicon particles.

Fig. 20. A series of pictures showing the correlation of a high silicon particle concentration and the resultant high density of linear etch pits.

Fig. 21. Schematic showing the "layering" of {111} in the sphalerite structure (after Hornstra[3]).

Fig. 22. Schematic of possible configuration of the "bottom" of a silicon deposit in a gallium arsenide matrix. The {111} are projected into the gallium arsenide matrix, indicating possible slip planes.

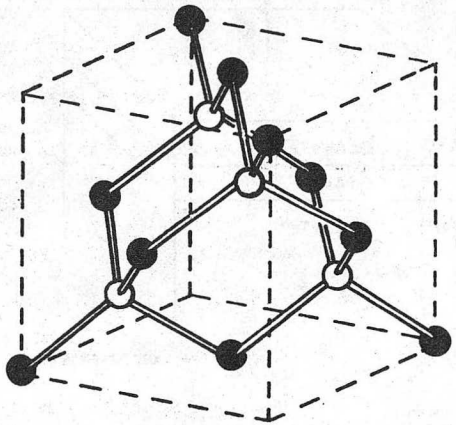

● GALLIUM
○ ARSENIC

XBL 716-6819

Fig. 1

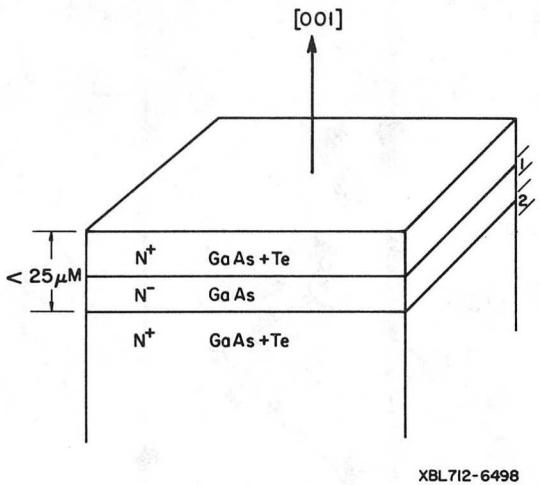

Fig. 2

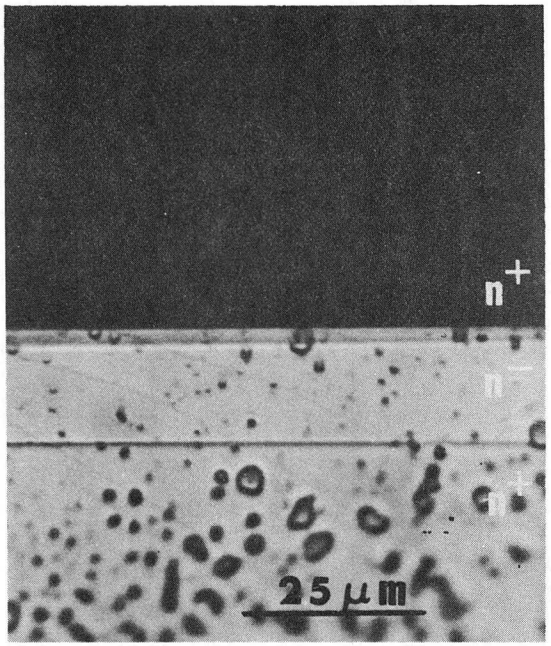

XBB 715-2200

Fig. 3

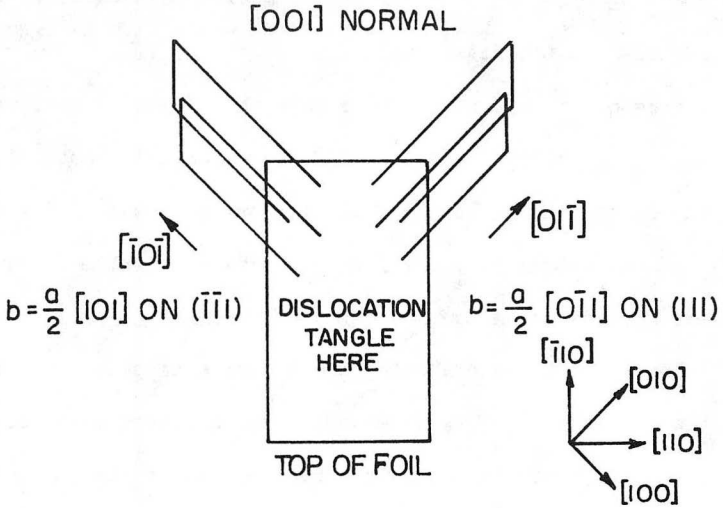

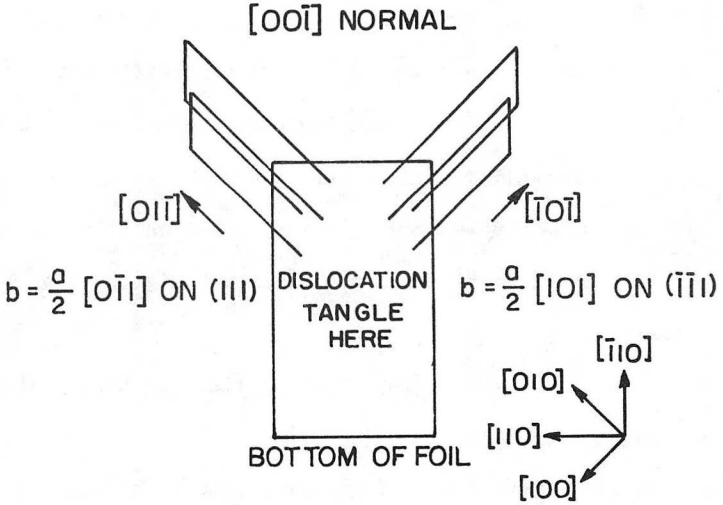

XBL716-6792

Fig. 4

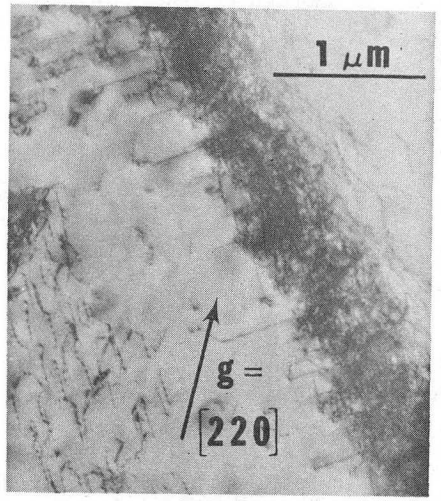

XBB 716-2377

Fig. 5

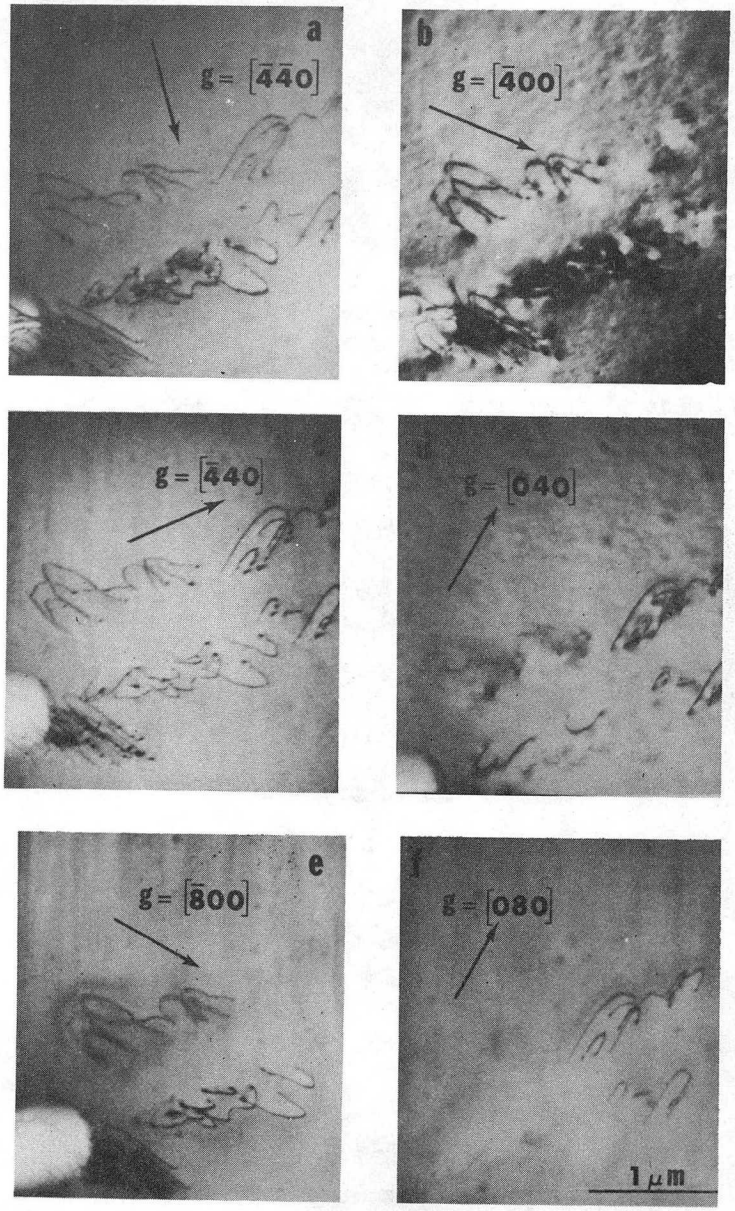

XBB 716-2383

Fig. 6

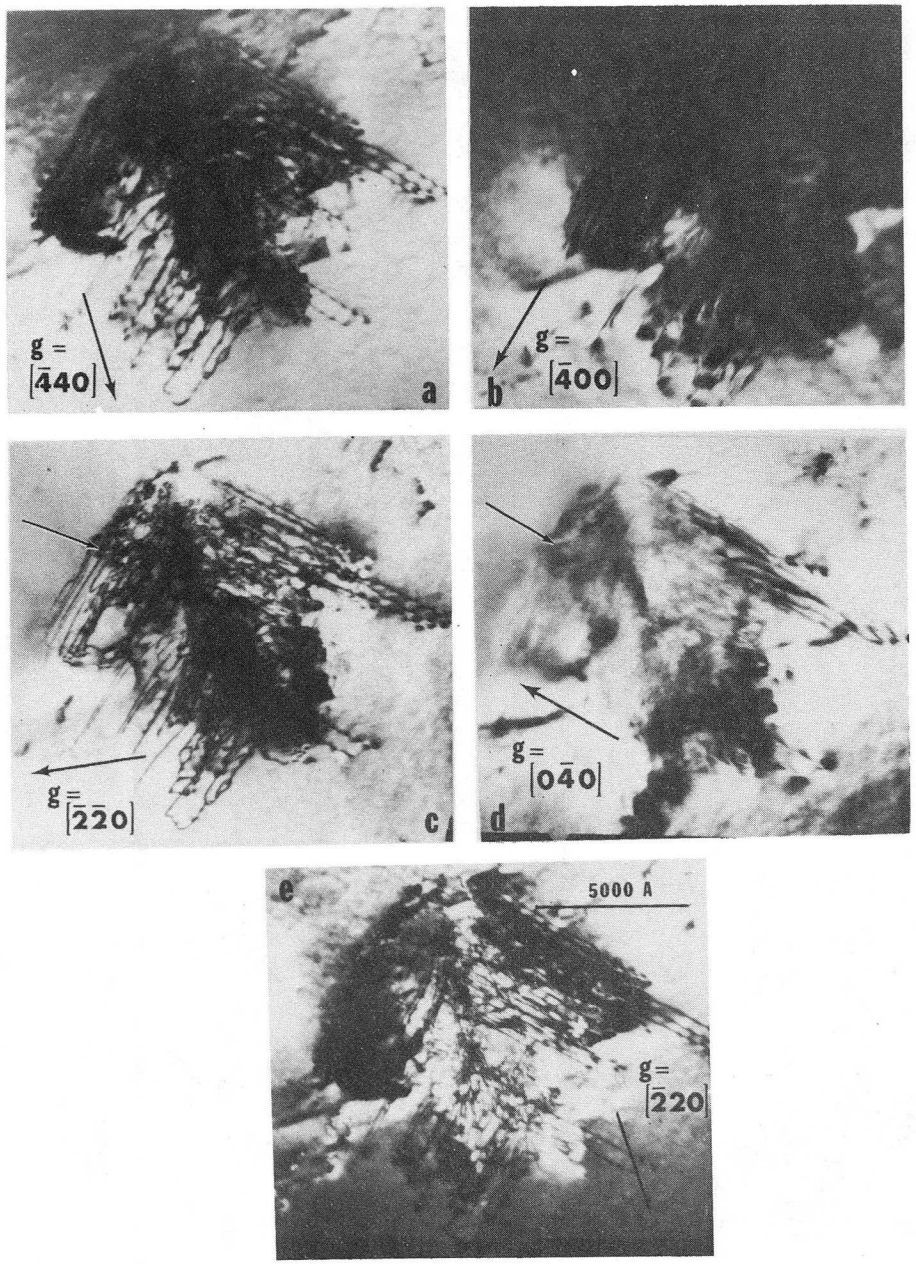

XBB 716-2380

Fig. 7

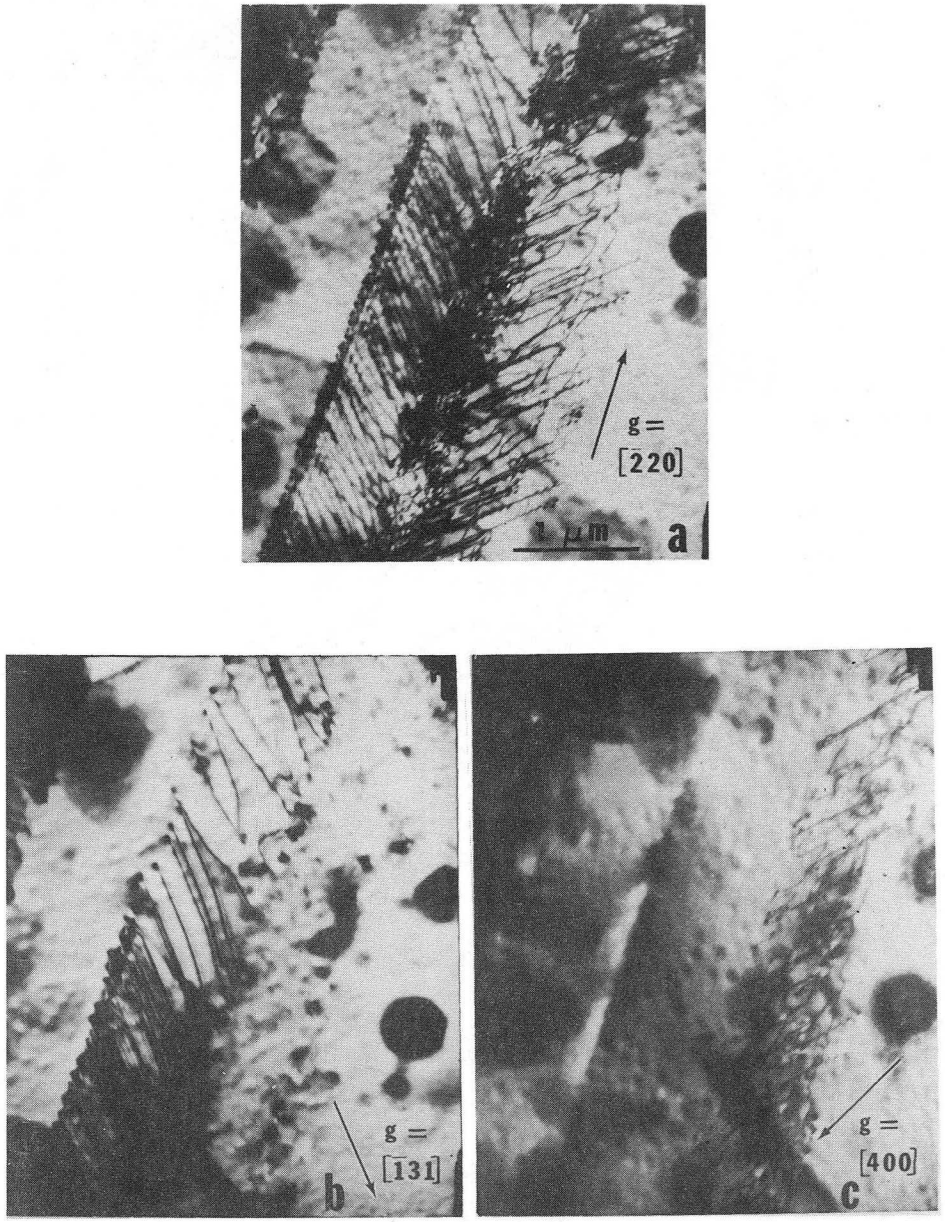

XBB 716-2386

Fig. 8

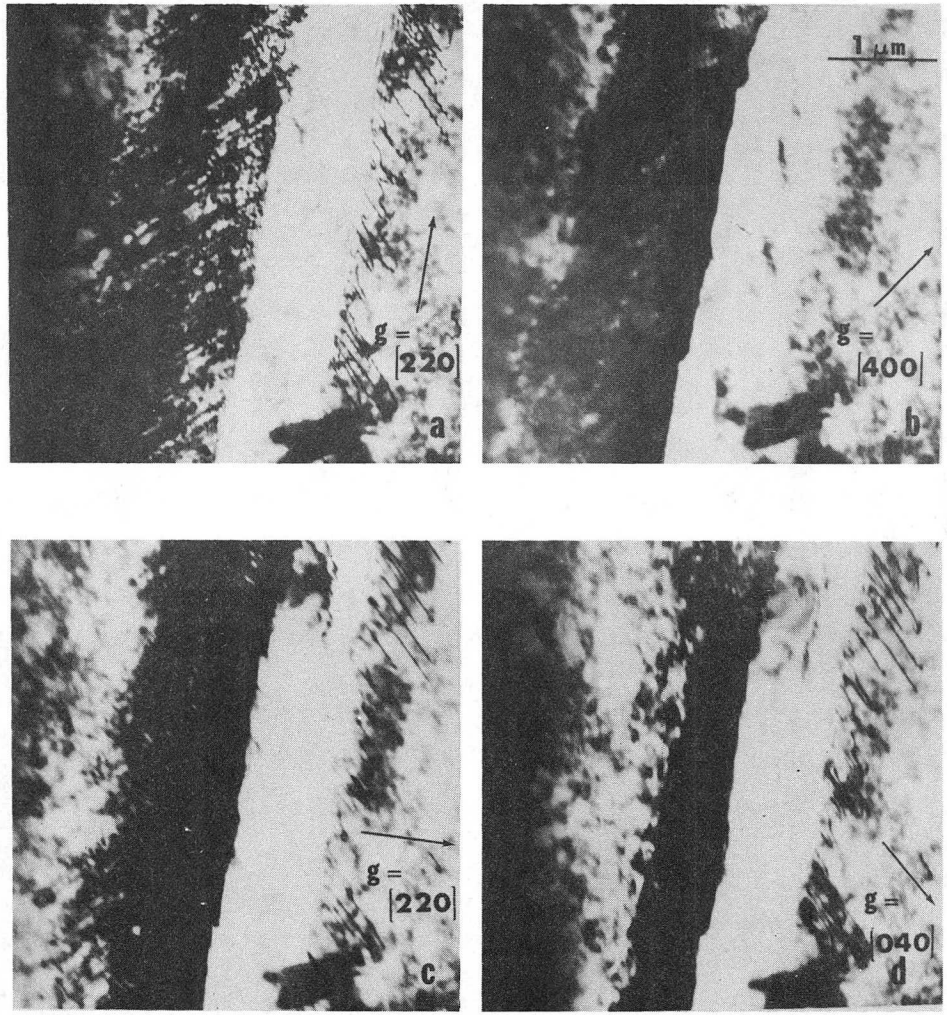

XBB 716-2379

Fig. 9

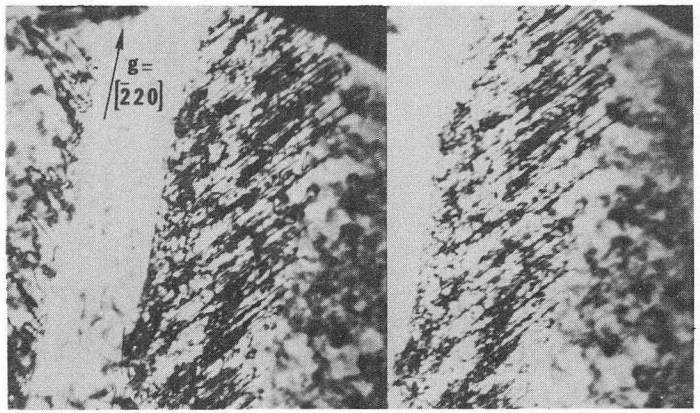

XBB 716-2378

Fig. 10

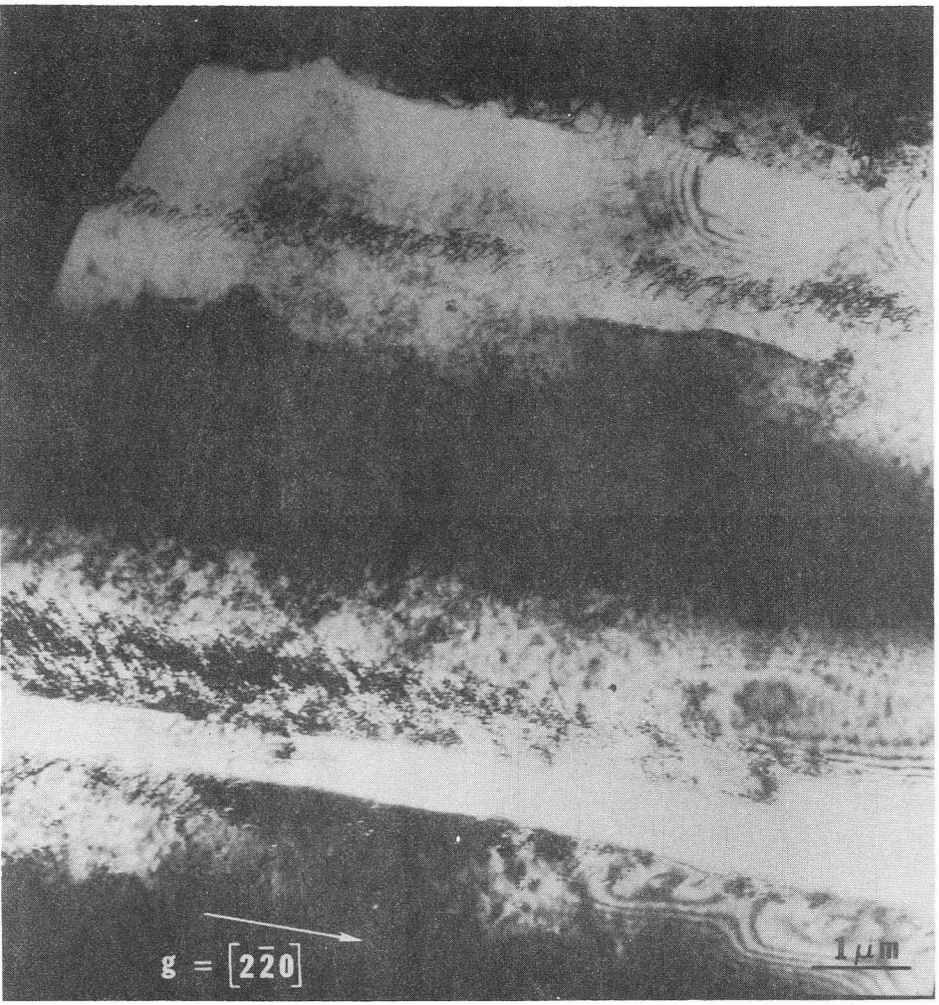

XBB 716-2388

Fig. 11

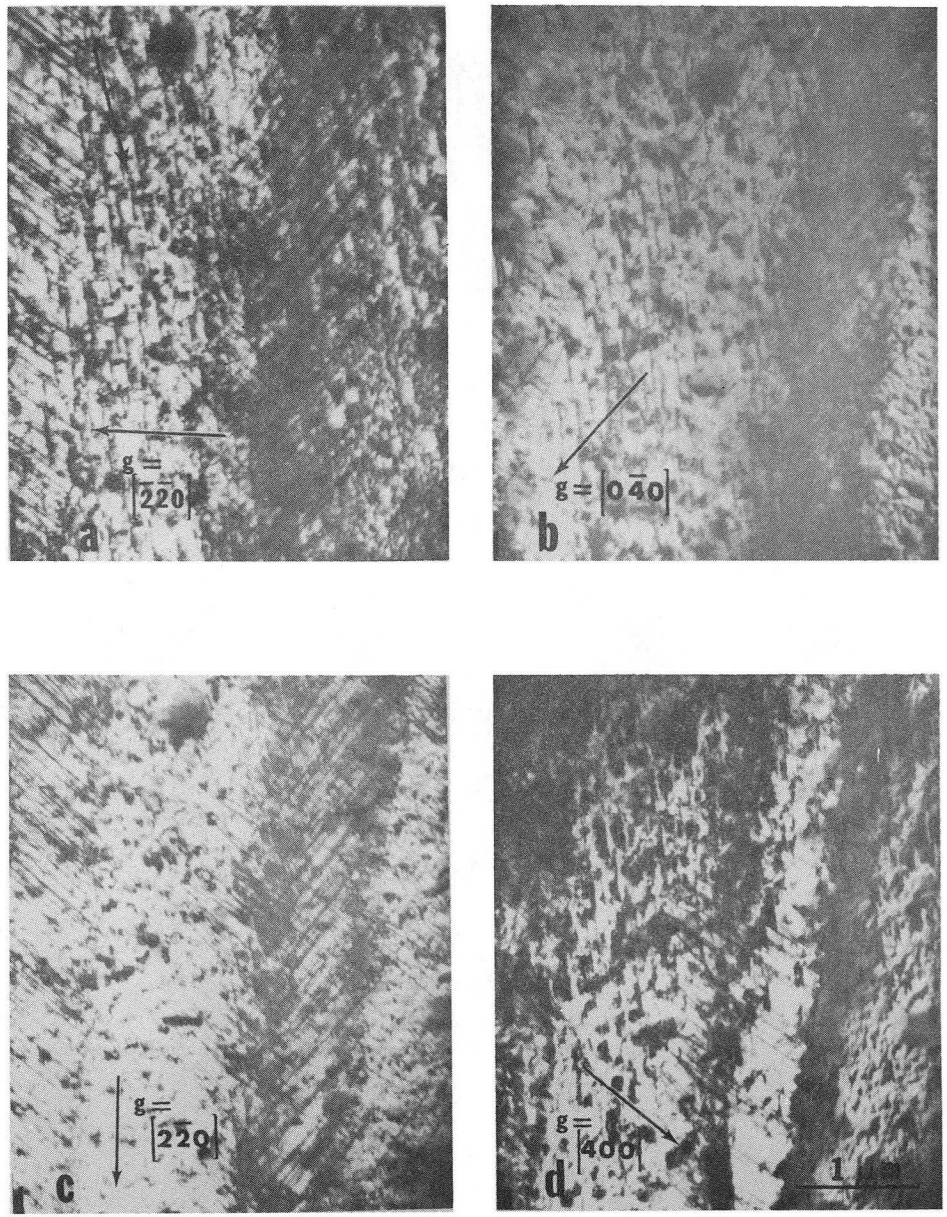

XBB 716-2381

Fig. 12

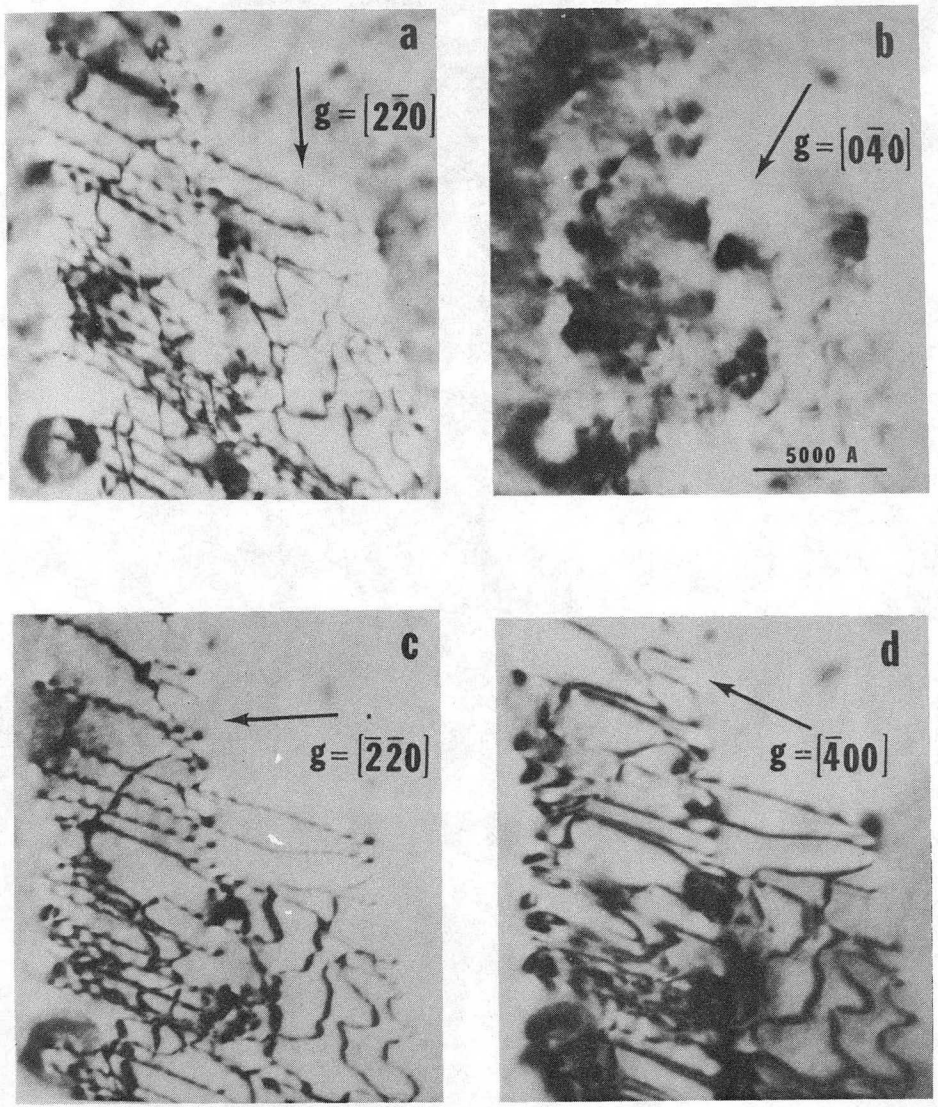

XBB 716-2385

Fig. 13

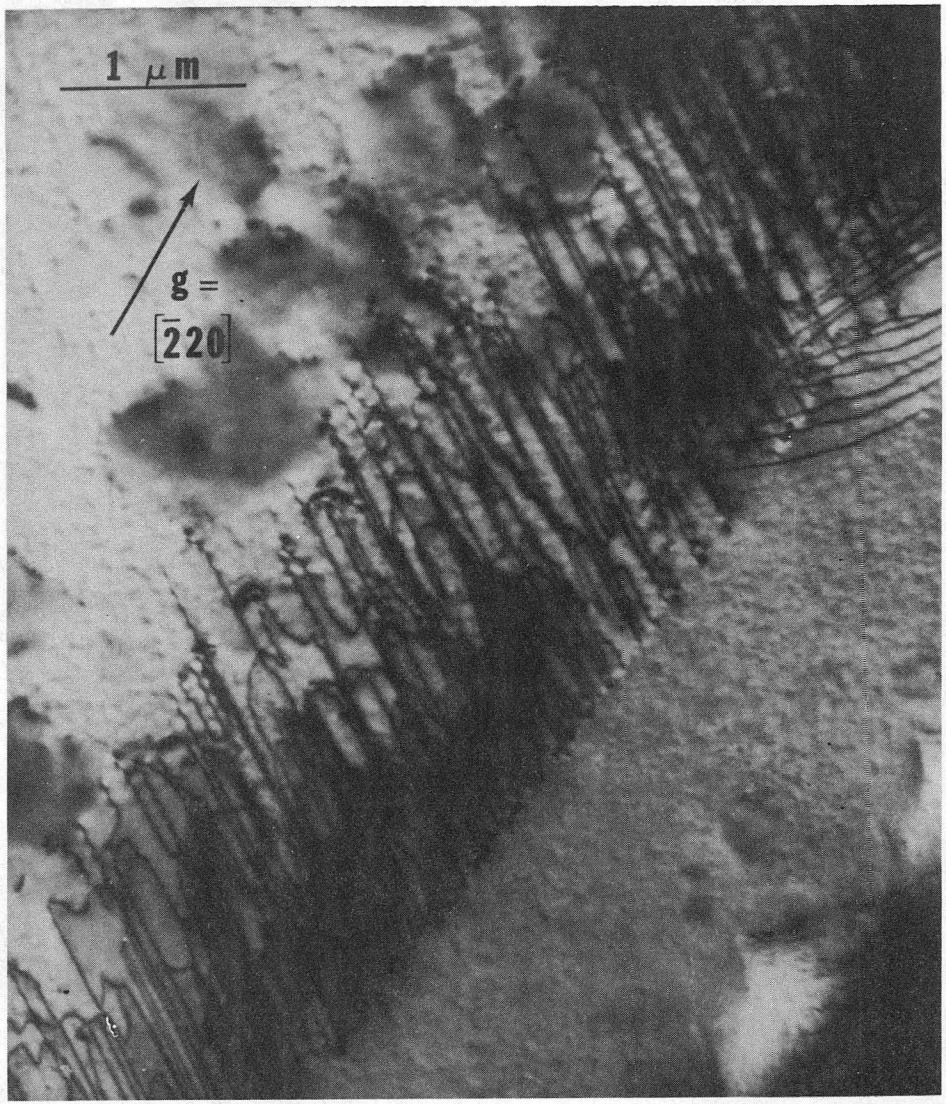

XBB 716-2387

Fig. 14

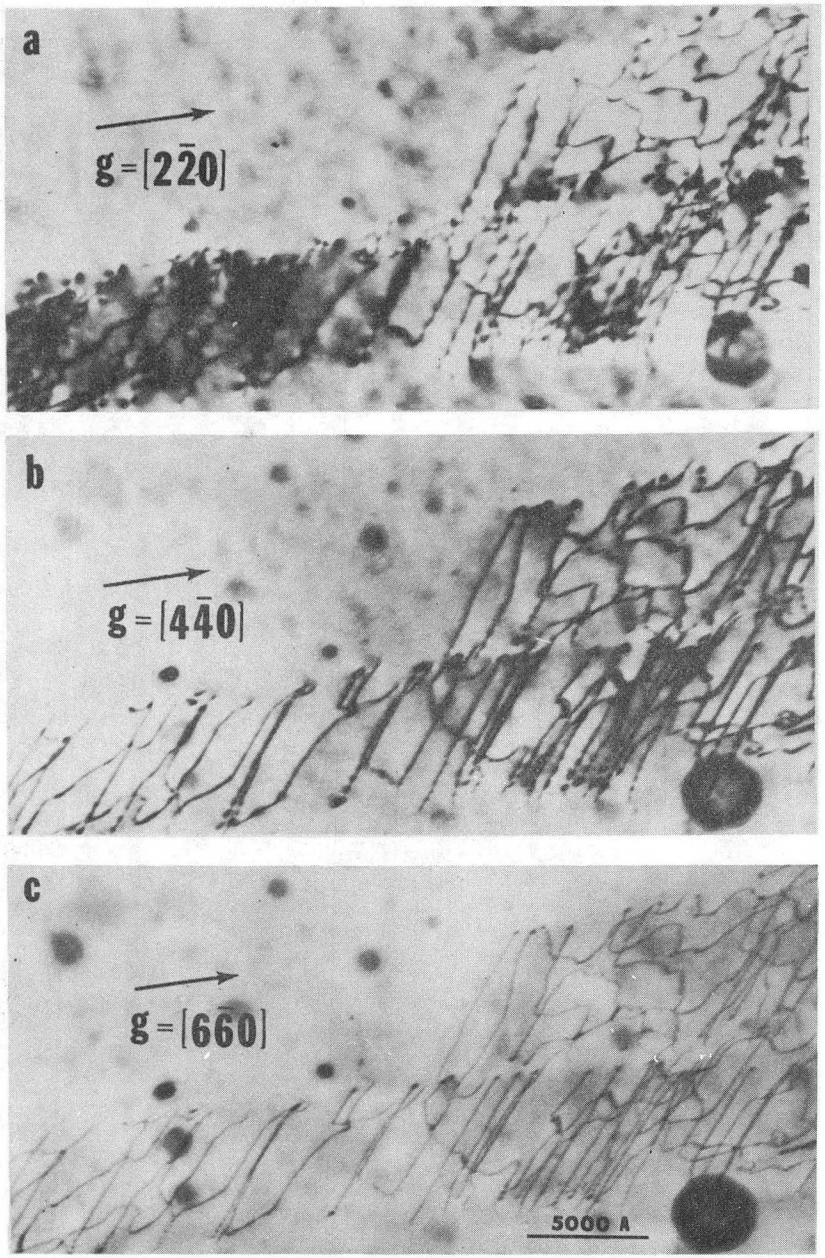

XBB 716-2384

Fig. 15

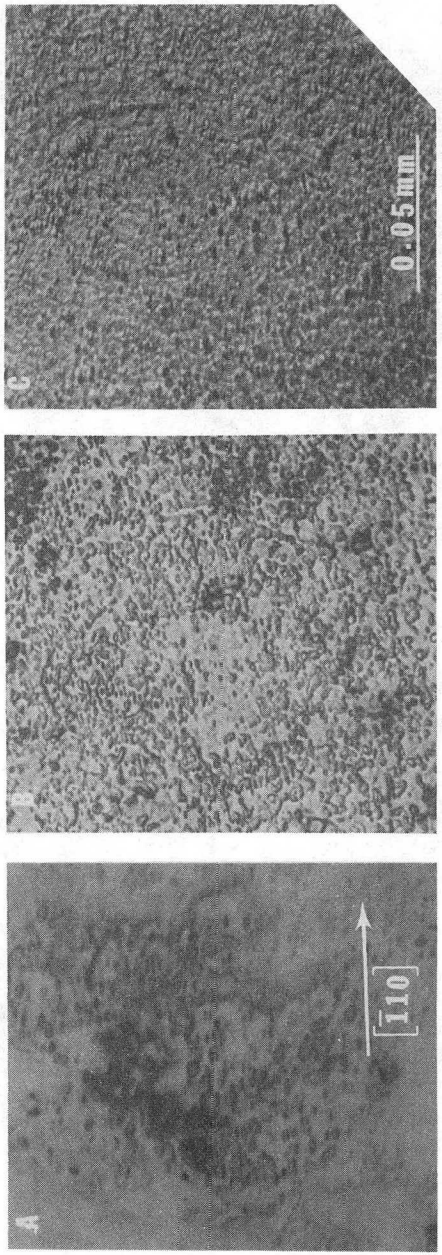

XBB 715-2201

Fig. 16

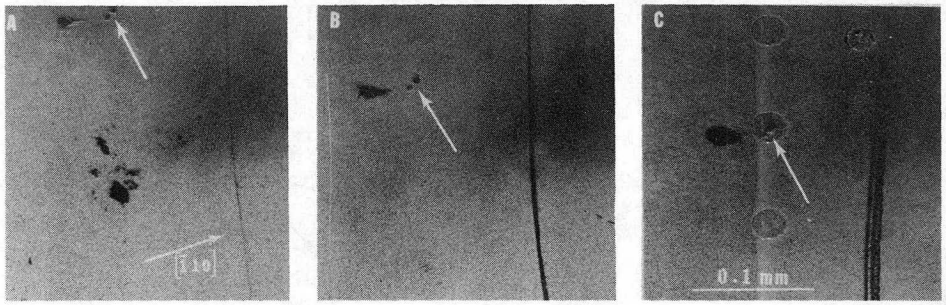

Fig. 17

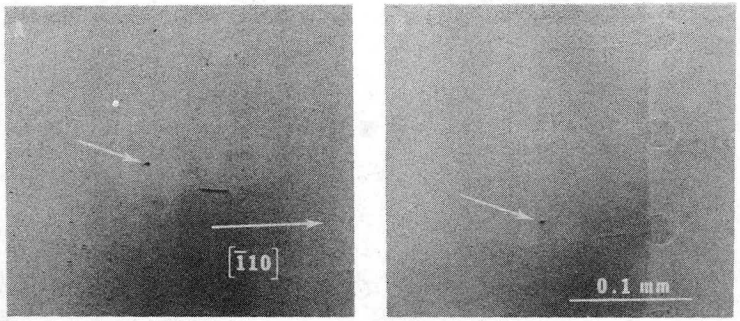

XBB 715-2202

Fig. 18

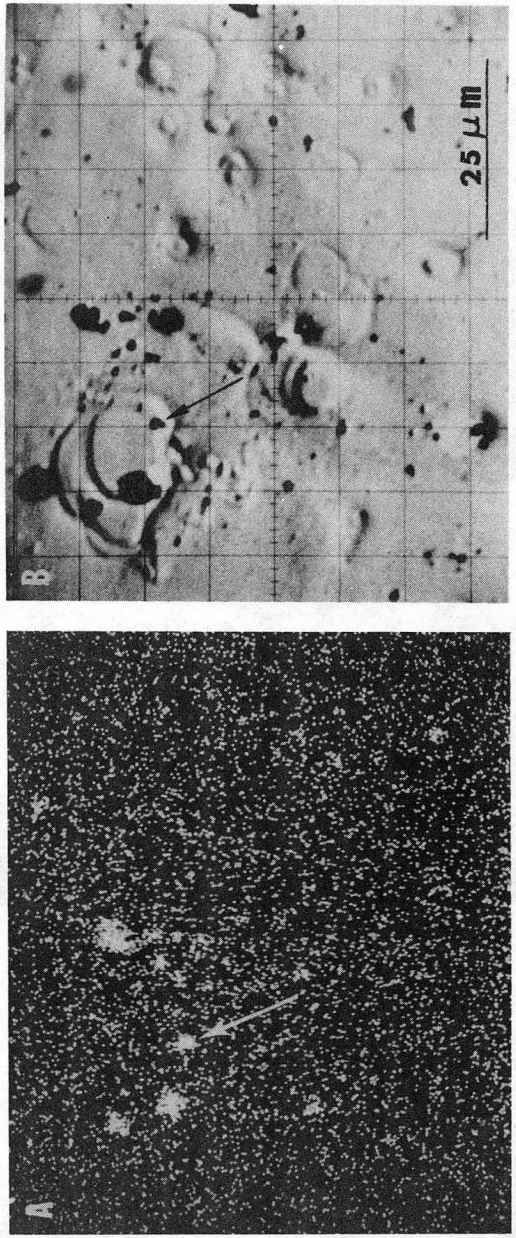

XBB 715-2204

Fig. 19

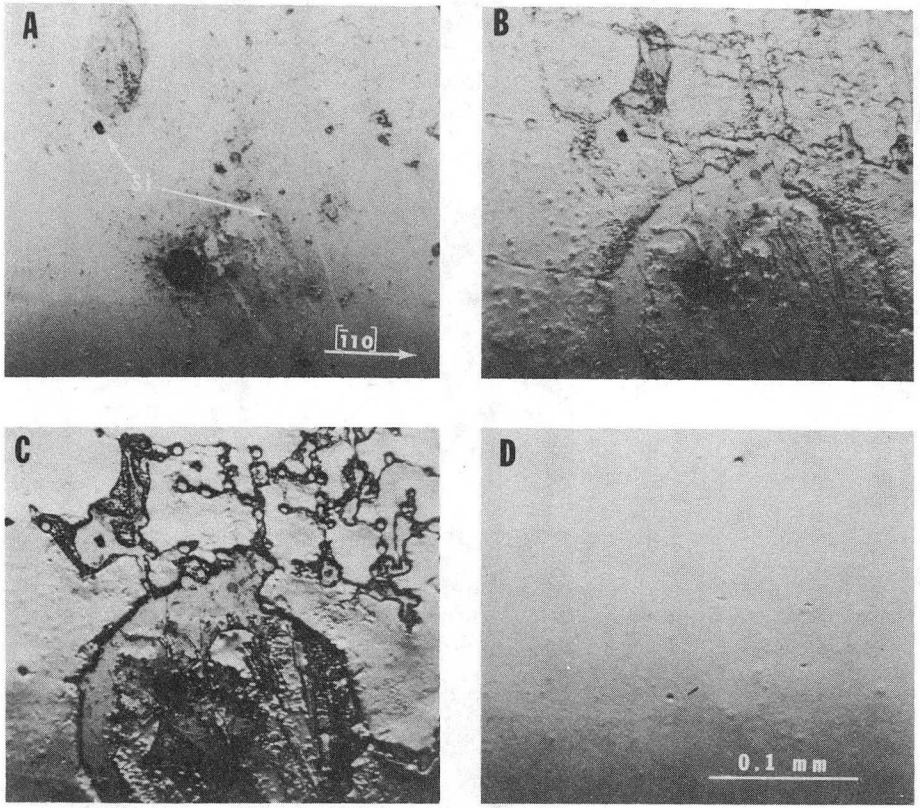

XBB 715-2203

Fig. 20

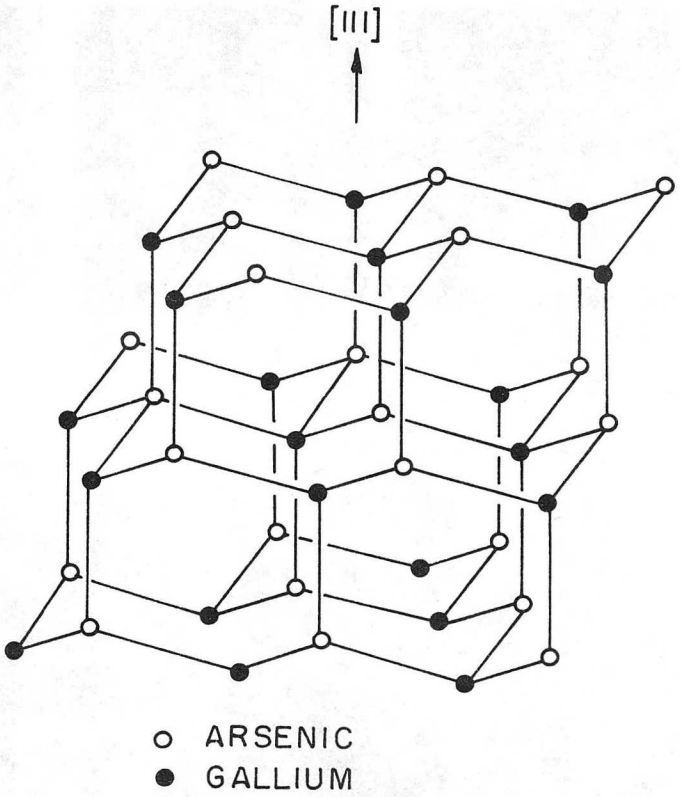

XBL716-6793

Fig. 21

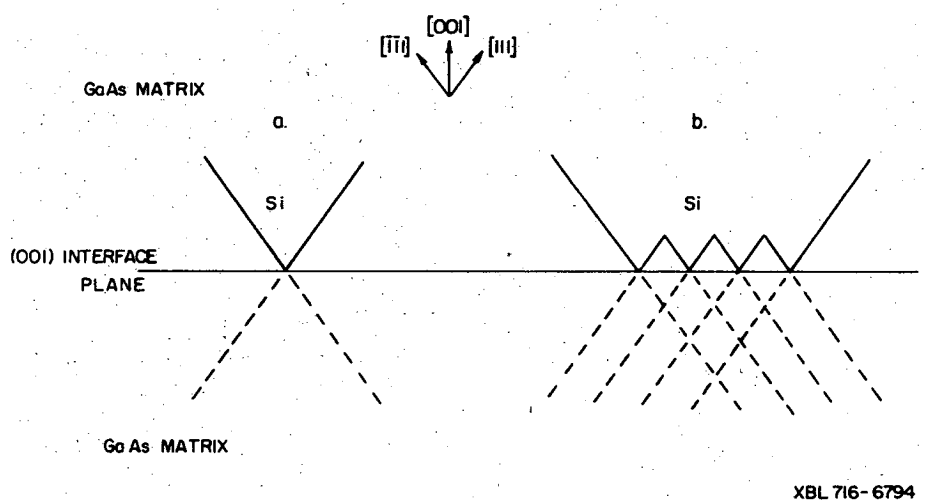

Fig. 22

APPENDIX

Negative resistivity is the term given to the characteristic of some materials which exhibit a decrease of electron drift velocity with increasing voltage. Gallium arsenide is one of the materials.

A plot of the carrier drift velocity (CDV) vs electric field (EF) for GaAs is shown in Fig. A-1. It can be seen that above a certain critical value of the electric field (the threshold ≅ 3000 v/cm × length) the drift velocity of the electrons decreases with increasing field, while below the threshold, the electrons behave "normally."

A model explaining this phenomenon is shown in Fig. A-2. This two-valley model compares the energy and instantaneous velocity of the electrons with the wave number K. It can be seen that the electrons can be excited into a higher energy "valley" where the mobility of the electrons is low. An increase in the energy of 0.35 eV is sufficient to excite an electron into this low mobility valley. Thus as the applied electric field is increased, more electrons are excited into a low mobility state with the result that the average drift velocity decreases.

This phenomenon is responsible for the "Gunn Effect" and is used in pulse generating devices as shown in Fig. 1 of the thesis. By applying an electric field across the electrically active (n^-) layer, electron flow is initiated. When above the threshold value, the electric field excites the electrons into the low mobility mode. This slowing down causes the electrons to "bunch up" forming a negative space charge or "domain." This domain drifts across the active region at a constant velocity ($\sim 10^7$ cm/sec).

When it reaches the high conductivity (n^+) anode, it dissipates, creating a "pulse" of current. Then another domain forms at the cathode and repeats this cycle.

Because of the constant drift velocity of the domains, it is possible to control the frequency of the pulses by varying the width of the active layer. By this means, it is possible to make pulse generating devices in the GHz range.

For more details, the reader is referred to reference 1.

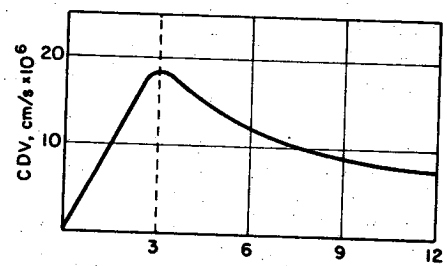

Fig. 1 A

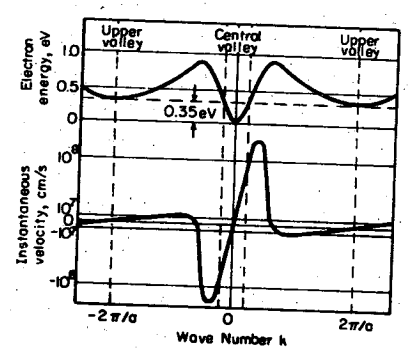

Fig. 2 A

XBL 716-6823

LEGAL NOTICE

This report was prepared as an account of work sponsored by the United States Government. Neither the United States nor the United States Atomic Energy Commission, nor any of their employees, nor any of their contractors, subcontractors, or their employees, makes any warranty, express or implied, or assumes any legal liability or responsibility for the accuracy, completeness or usefulness of any information, apparatus, product or process disclosed, or represents that its use would not infringe privately owned rights.

TECHNICAL INFORMATION DIVISION
LAWRENCE RADIATION LABORATORY
UNIVERSITY OF CALIFORNIA
BERKELEY, CALIFORNIA 94720